

Fig S1. CSR-1/22G targets proteasome subunits. **a** Summary of CLASH data processing (Supplementary Table S1). **b** Nucleotide analysis. Analysis for the length and first nucleotide distribution biases of CSR-1 bounded small RNAs. **c** Distribution of small RNA cleavage sites on *rpn-9* identified by CLASH. Sequences and base pairing chimeras are shown. **d** Phenotype enrichment analysis using the CSR-1 CLASH identified targets gene set. Number in each bar represents the counts of genes enriched in each term. **e** Protein-protein interaction network and MCODE components identified in embryonic lethality related CSR-1 targets. The size of a protein circle refers to the number of direct interactions that reveal functional importance. **f** Representative immunoblots of indicated protein levels of *C. elegans* (*rpn-12::2×flag*, *3×flag::F35G12.12*, *3×flag::rpt-6*, *3×flag::pas-1*, *3×flag::pbs-1*, *pas-2::2×flag*) germ cells. Tubulin serves as loading control. * Labeled blots indicate the genes showed no increase of protein and mRNA levels in *csr-1* depletion. **g** Representative images of *rpn-12* RNA FISH and quantification of fluorescence signal in the last five oocytes for the indicated conditions. Scale bars = 50 μ m. Results of n = 10 replicates are shown, data are represented as mean \pm SD. **P < 0.01. **h** RPN-12 immunofluorescence (*2×flag::rpn-12*) and quantification of fluorescence signal in the last five oocytes for the indicated conditions. Scale bars = 50 μ m. Results of n = 10 replicates are shown, data are represented as mean \pm SD. **P < 0.01. **i** Quantification of relative assembling levels of the 19S, 20S, and 26S proteasomes. Results of n = 3 replicate experiments are shown, data are represented as mean \pm SD. *P < 0.05, ***P < 0.001, no significant (ns). **j** Chymotrypsin-like, caspase-like, and trypsin-like proteasome activities (relative slope to control RNAi without 0.02% SDS are shown. Results of n = 3 replicate experiments are shown, data are represented as mean \pm SD. *P < 0.05, ***P < 0.001, no significant (ns).

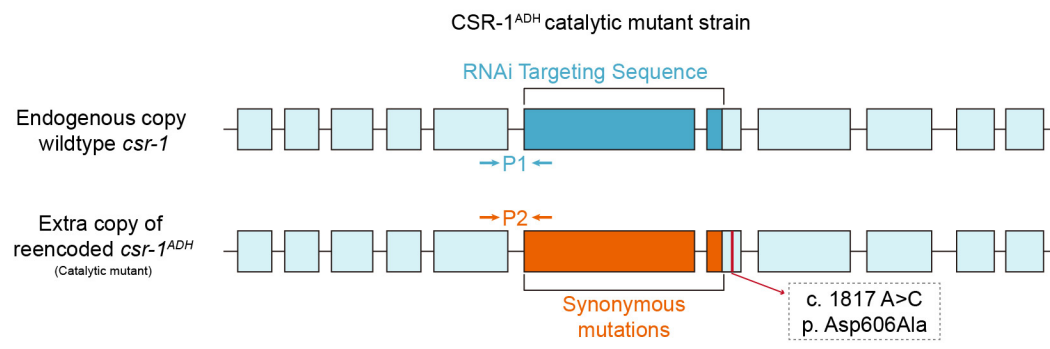
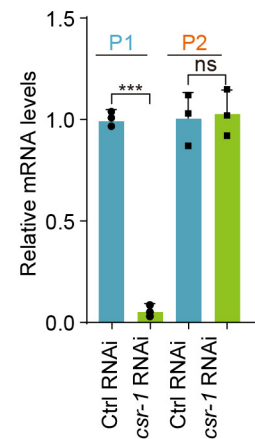
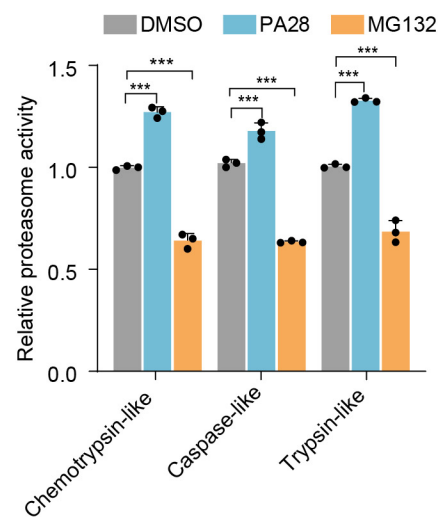
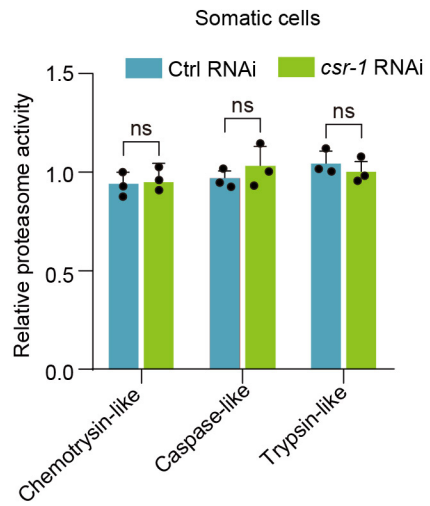
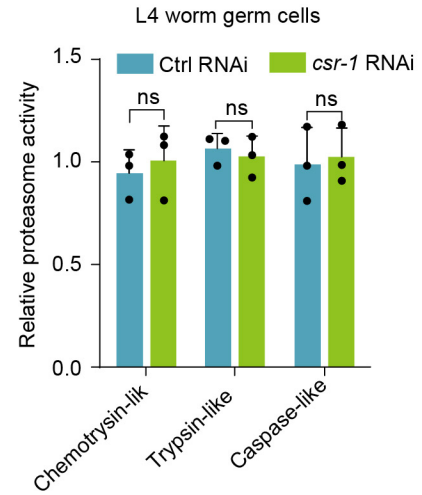
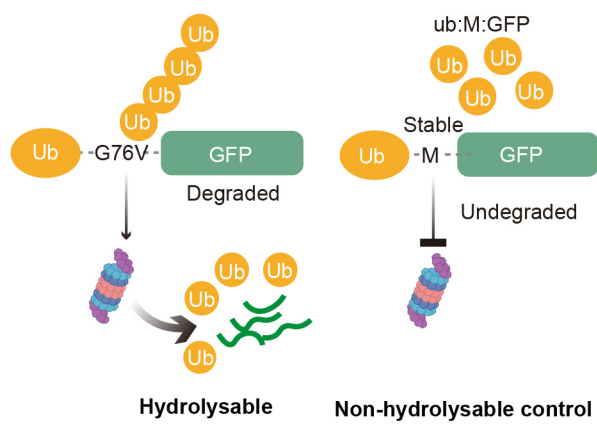
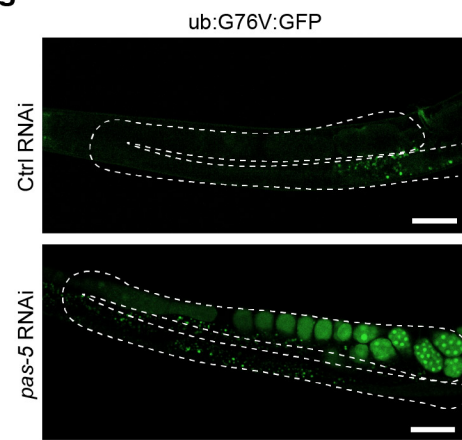
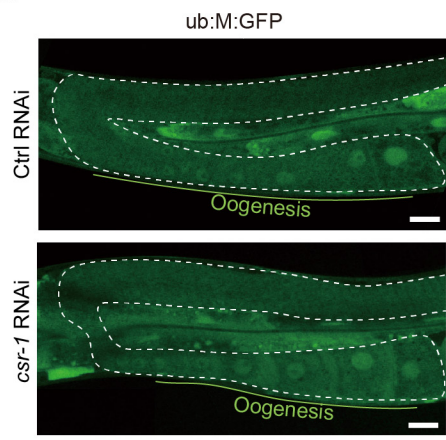
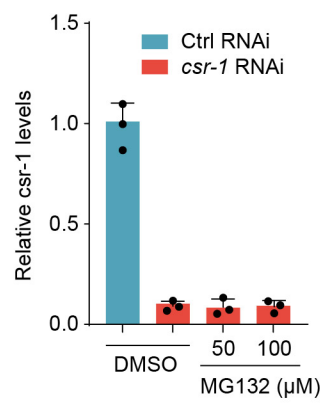
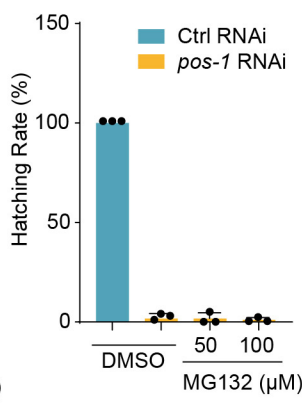
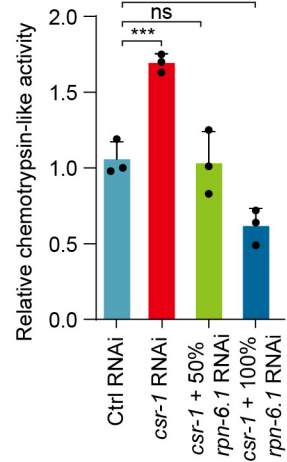
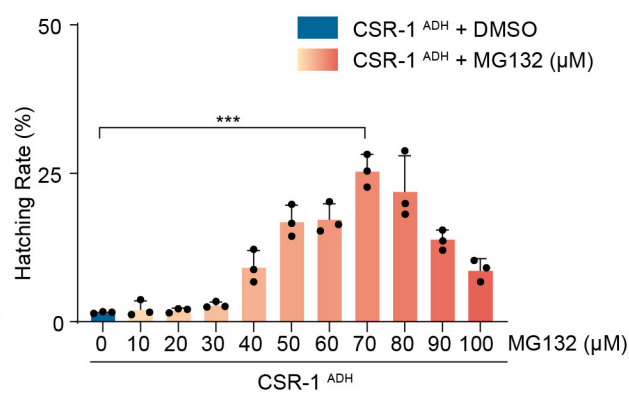
a**b****c****d****e****f****g****h****i****j****k****l**

Fig S2. CSR-1 affects proteasome activity in oocytes of *C. elegans*. **a** Schematic diagram of the CSR-1 catalytic mutant strain generation. **b** qPCR results of the expression levels of catalytic mutation *csr-1^{ADH}* with specific primers designed for wildtype sequence (P1) and synonymous mutation sequence (P2). **c** Proteasome activities (relative slope to DMSO) of worm lysis incubated with PA28 and MG132 are shown. Results of n = 3 replicate experiments are shown, data are represented as mean \pm SD. ***P < 0.001. **d** Proteasome activities (relative slope to control RNAi) in *C. elegans* somatic cells are shown. Results of n = 3 replicate experiments are shown, data are represented as mean \pm SD. No significant (ns). **e** Proteasome activities (relative slope to control RNAi) in germ cells of L4 *C. elegans* are shown. Results of n = 3 replicate experiments are shown, data are represented as mean \pm SD. No significant (ns). **f** Schematic diagram of ubiquitin-based GFP tagging system for proteasome activity assay in vivo. **g** Representative images of GFP signal of the in vivo hydrolysable GFP reporter (*ub::G76V::gfp*) for *pas-5* RNAi. Scale bars = 100 μ m. **h** Representative images of GFP signal of the in vivo non-hydrolysable GFP reporter (*ub::M::gfp*) for control and *csr-1* RNAi. Scale bars = 20 μ m. **i and j** Effectiveness of RNAi after MG132 treatment is shown by (i) analysis of *csr-1* mRNA levels and (j) embryonic viability analysis by *pos-1* RNAi. Results of n = 3 replicate experiments are shown. Embryos from more than 20 P0 worms were counted for each replicate. Data are represented as mean \pm SD. ***P < 0.001, no significant (ns). **l** Embryo hatching rates were calculated for gradient concentration of MG132 treatment in the background of CSR-1^{ADH}. Results of n = 3 replicate experiments are shown, data are represented as mean \pm SD. Embryos from more than 20 P0 worms were counted for each replicate. ***P < 0.001.

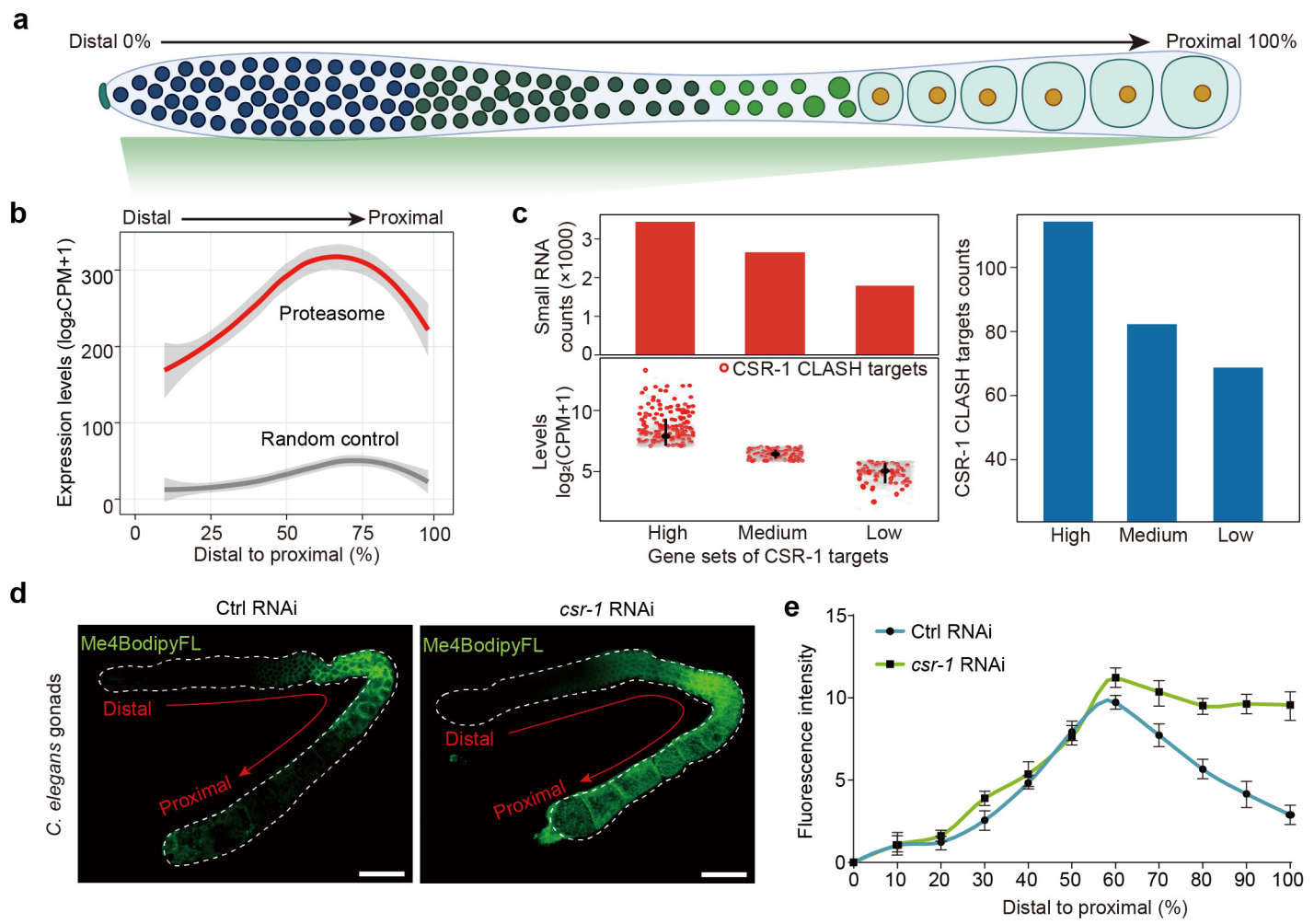


Fig S3. Dynamic proteasome activities in germ cell development. **a** Schematic diagram of the *C. elegans* germline. **b** Spatial expression of proteasome transcripts from distal to proximal. **c** CSR-1 targets with different expression levels are divided into 3 groups (Low, Medium, High; lower left), CLASH identified CSR-1 cleaved targets were indicated in red circles and the counts are shown on the right, targeting small RNA levels in each group are shown on upper left. **d and e** Representative images (d) and quantification (e) of Me4bodiFL signal in *C. elegans* gonads. Scale bars = 40 μ m. Results of n = 3 replicate experiments are shown, data are represented as mean \pm SD.

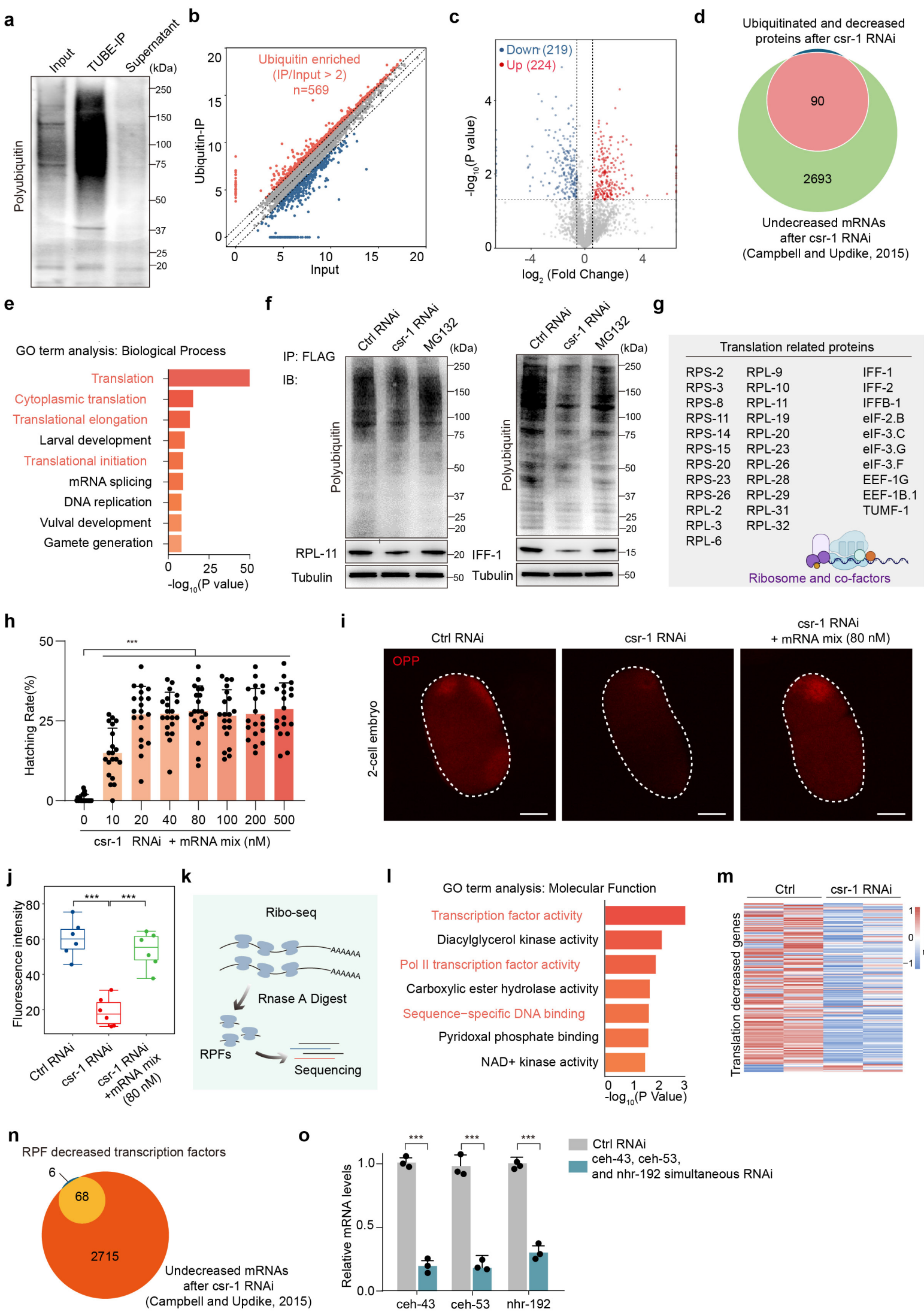


Fig S4. Proteasome regulates the degradation of translation proteins. **a** Representative immunoblots of different fractions from TUBEs pulldown assay. **b** Scatter plots showing the TUBEs pulldown polyubiquitinated proteins compared to input. An enrichment of IP/input > 2 is used as cutoff. **c** Volcano plots showing LC-MS/MS results that differentially expressed proteins identified in *csr-1* RNAi germ cells compared to control RNAi. Fold change (FC) of 1.5 and p value of 0.05 are used as cutoff. **d** Venn diagram showing the overlap between proteasome targets we identified and mRNA levels unchanged gene lists. **e** GO term analysis using the identified ubiquitin-proteasome degraded proteins. **f** Immunoblots of anti-FLAG co-IP (*rpl-11::3×flag* and *iff-1::3×flag*). Tubulin serves as input loading control. **g** Identified proteasome targets of translation genes. **h** Embryo hatching rates were calculated for indicated conditions. Results of n = 20 worms are shown, data are represented as mean ± SD. ***P < 0.001. **i and j** Representative (i) fluorescent images and (j) quantification of OPP assay with 2-cell embryos from control, *csr-1* knockdown, and *csr-1* knockdown with translational mRNA injection *C. elegans*. Scale bars = 10 μm. Results of n = 6 replicate experiments are shown, each replicate was analyzed with more than 20 embryos, data are represented as mean ± SD. ***P < 0.001. **k** Schematic diagram of Ribo-lite sequencing. **l** GO term analysis using the RPFs decreased gene list in *csr-1* knockdown germ cells. **m** Heatmap showing the protein abundance of genes with reduced translation efficiency in the indicated groups. **n** Venn diagram showing the overlap between transcription factors with reduced translation efficiency and genes with unchanged mRNA levels.. **o** qPCR analysis showing mRNA levels of *ceh-43*, *ceh-53*, and *nhr-192* in *C. elegans* germ cells. Results of n = 3 replicate experiments are shown, data are represented as mean ± SD. ***P < 0.001.

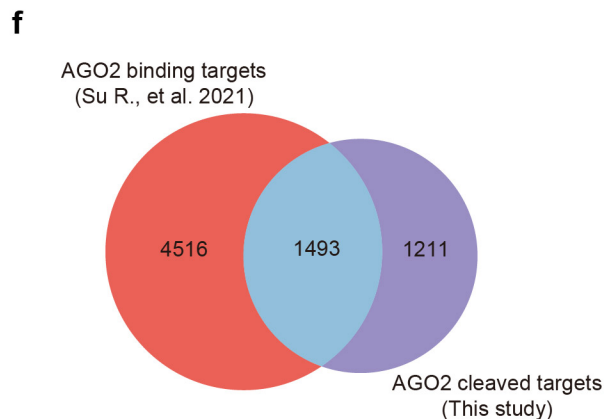
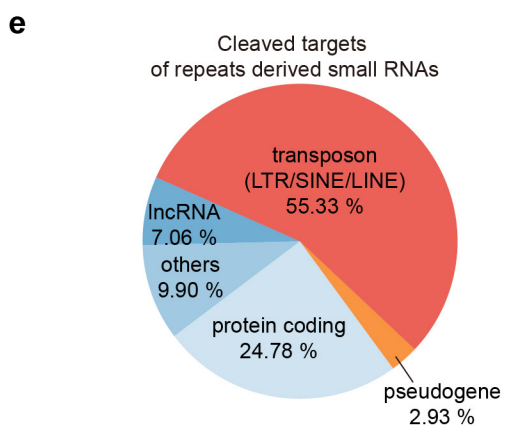
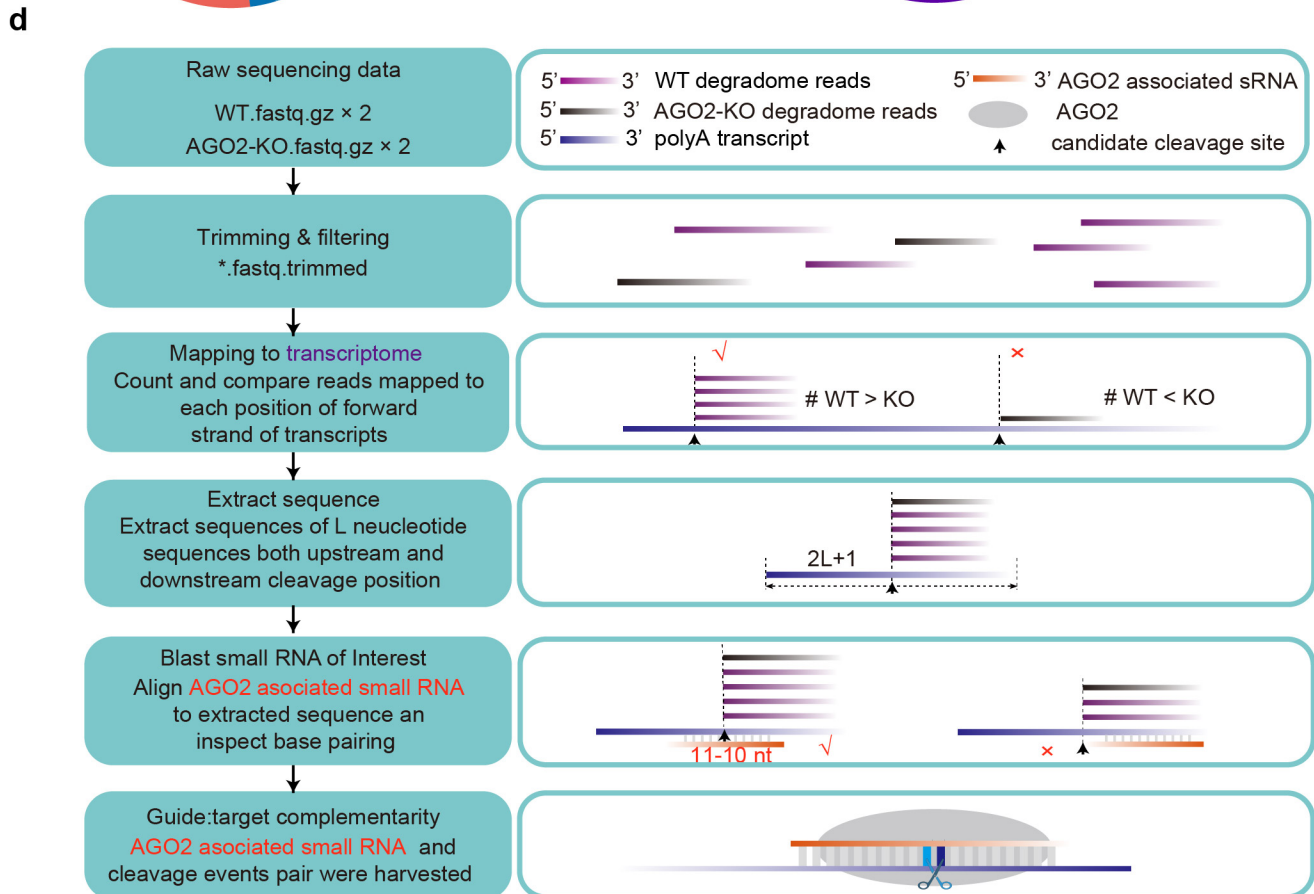
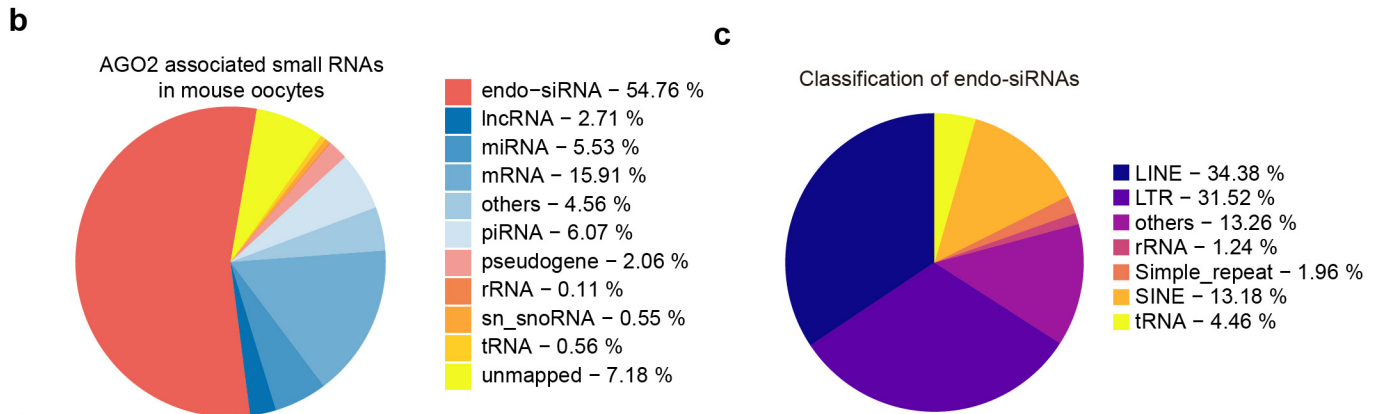
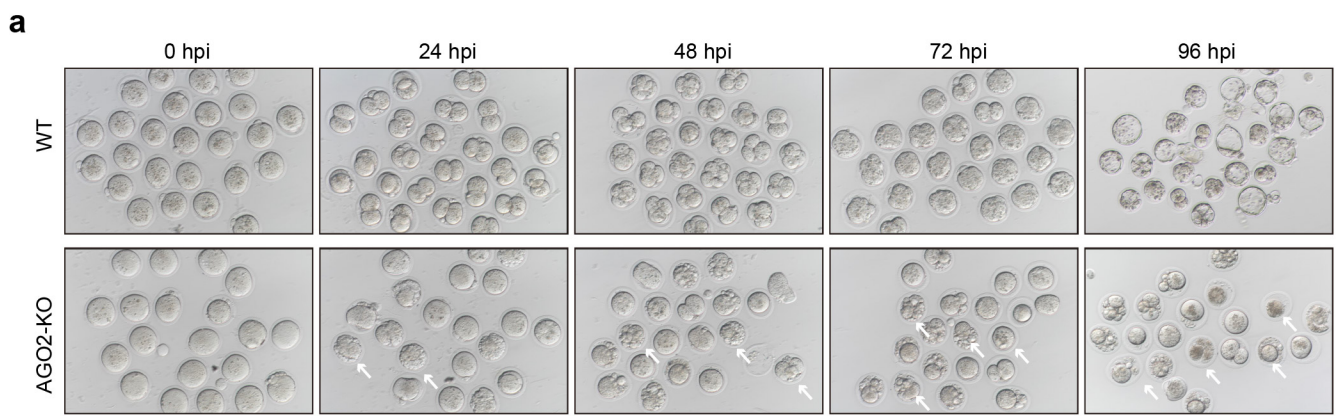


Fig S5. AGO2 is largely loaded with endo-siRNAs in mouse oocytes. **a** Representative image of in vitro fertilization results from wildtype and AGO2 knockout oocytes. Fertilized AGO2 knockout oocytes are blocked at the 1-2 cell embryo stage. White arrows show the representative dead embryos. **b** Pie charts showing the percentage of the classification about AGO2 associated small RNAs. **c** Pie charts showing the percentage of the biogenesis classification of endo-siRNAs identified by CAS-sequencing. **d** Schematic diagram of the analysis strategy to identify the AGO2/small RNA targets in oocytes. **e** Pie charts showing the percentage of repeats-derived small RNA cleaved targets identified in mouse oocytes. **f** Venn diagram illustrates the overlap of AGO2 target genes identified by LACE-seq and by degradome-seq in this study.

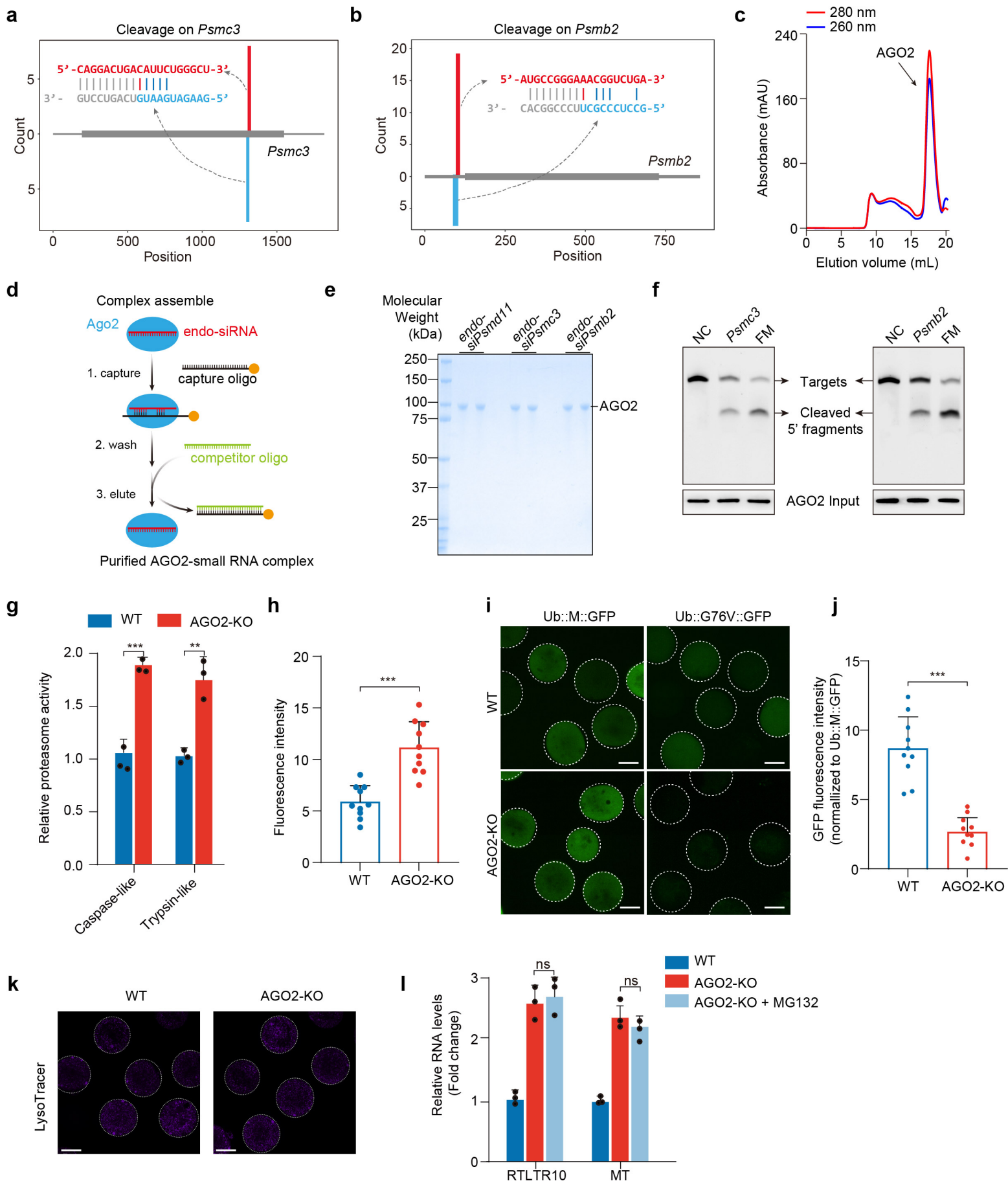


Fig S6. AGO2/endo-siRNAs cleave proteasome mRNAs. a and b Distribution of small RNA reads (red) identified by AGO2-IP small RNA sequencing, and the distribution of target *Psmc3* (a) and *Psmb2* (b) mRNA reads (blue) identified by degradome sequencing. Sequences and base pairing of small RNA:*Psmc3* and small RNA:*Psmb2* are shown. **c** Size-exclusion chromatography profile of the purified AGO2 proteins (arrow). **d** Schematic diagram of AGO2-small RNA complex purification workflow. **e** SDS-PAGE analysis of the purified AGO2-small RNA complex. **f** Representative urea-PAGE showing AGO2-mediated cleavage of 5'-FAM-labeled *Psmc3*, *Psmb2* mRNA target site sequence, fully matched (FM) target RNAs or non-complementary (NC) target RNAs. **g** Caspase-like and trypsin-like proteasome activities (relative slope to wildtype) in mouse oocytes are shown. Results of n = 3 replicate experiments are shown, each replicate was analyzed with more than 10 oocytes, data are represented as mean \pm SD. ***P < 0.001. **h** Quantification of Me4bodiFL signal in WT and AGO2-KO oocytes. Results of n = 10 replicate experiments are shown, data are represented as mean \pm SD. ***P < 0.001. **i and j** Representative images (i) and quantification (j) of GFP signal in the wildtype and AGO2-KO MII oocytes injection of *ub::G76V::gfp* and *ub::G76V::gfp* mRNAs. Scale bars = 50 μ m. Results of n = 10 replicates are shown, each replicate was analyzed with more than 10 oocytes, data are represented as mean \pm SD. ***P < 0.001. **k** Representative images of LysoTracker signals in oocytes. **l** qPCR analysis showing RNA levels of *RTLTR10* and *MT* in WT, AGO2-KO, and MG132 rescued oocytes. Results of n = 3 replicate experiments are shown, data are represented as mean \pm SD.

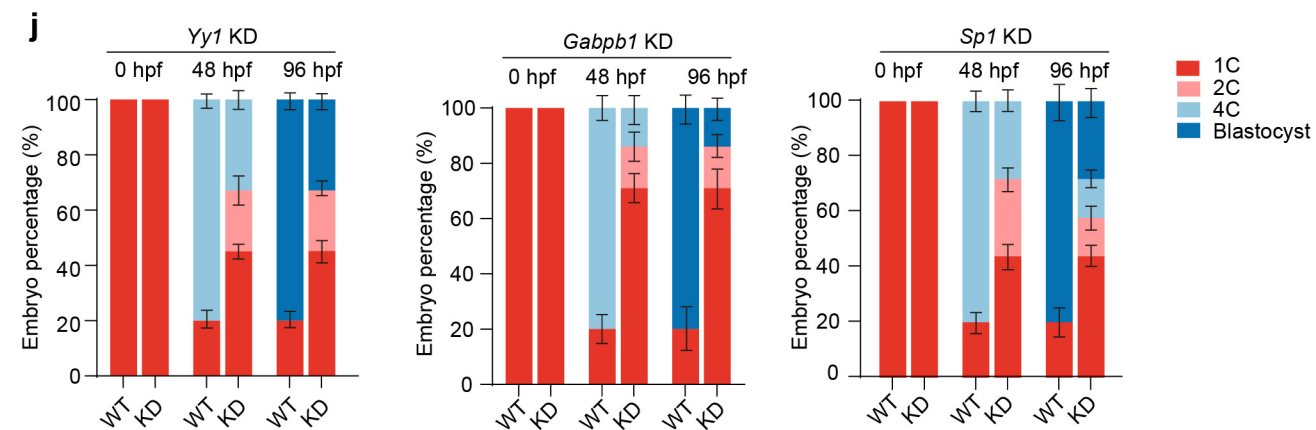


Fig S7. Proteasome mediates the degradation of ribosomes thus affect embryo development. **a** Scatter plots showing the TUBEs pulldown polyubiquitinated proteins compared to input. An enrichment of IP/input > 2 is used as cutoff. **b** Scatter plots showing the LC-MS/MS results that differentially expressed proteins in AGO2-KO MII oocytes compared to wildtype. Fold change (FC) of 1.5 is used as cutoff. **c** Venn diagram shows the counts of ubiquitinated proteins and level decreased proteins in AGO2-KO MII oocytes. **d** Venn diagram showing the overlap between proteasome targets we identified and expression unchanged mRNA gene lists. **e** GO term analysis of the proteasome targeting proteins. **f** Distribution of identified ubiquitinated sites in proteins of MII oocytes. **g** Scatter plots showing LC-MS/MS analysis of proteins encoded by translation-decreased genes in AGO2-KO MII oocytes compared with wild-type controls. Blue dots indicate proteins with reduced abundance. **h** qPCR analysis showing mRNA knockdown efficiency of siRNAs in mouse MII oocytes. Results of n = 3 replicate experiments are shown, data are represented as mean ± SD. ***P < 0.001. **i and j** Embryo morphology (i) and developmental rates (j) of negative control (NC) and indicated genes knockdown (KD) embryos in vivo. Sample sizes from three independent experiments are NC: n = 15, 12, and 13; *Gabpb1* KD: n = 14, 11, and 17; *Yyl* KD: n = 16, 13, and 20; *Sp1* KD: n = 13, 17, and 14.

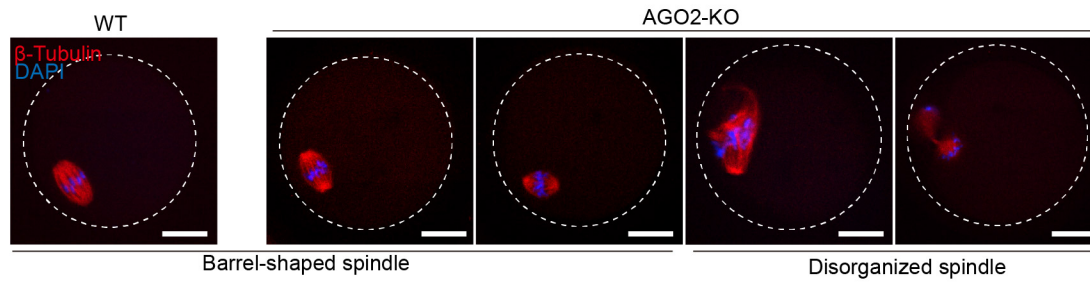
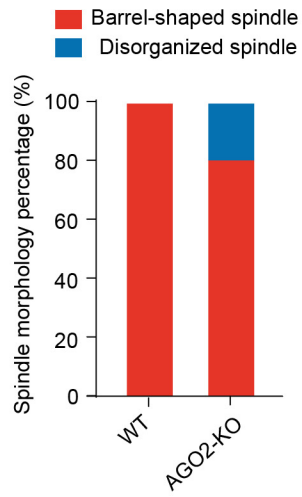
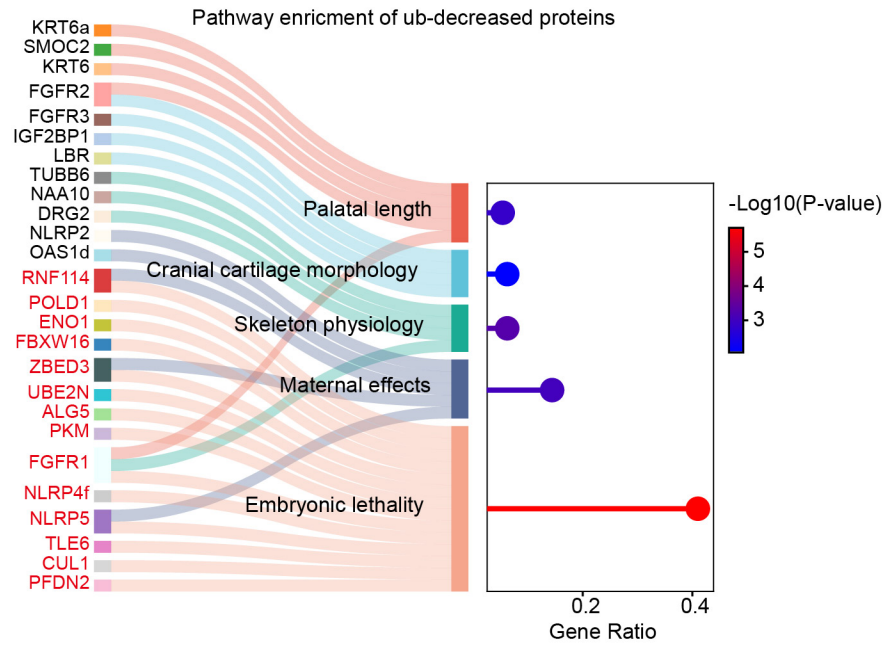
a**b****c**

Fig S8. Phenotypes induced by AGO2-KO in mouse oocytes. **a** Representative image of spindle morphology in wildtype and AGO2-KO MII oocytes. Microtubules were stained with an anti-tubulin (red) and DNA was stained with DAPI. Scale bars = 20 μ m. **b** Proportion of each type of spindle morphology in wildtype and AGO2-KO MII oocytes. Sample sizes for each group are WT: n = 50; AGO2-KO: n = 90. **c** Pathway enrichment of ubiquitinated proteins decreased in AGO2-KO oocytes. Sankey diagram on the left shows representative genes enriched in each pathway.